



Chaetoceros turingii sp. nov. (Bacillariophyceae): morphological and molecular description of a new species from the Gulf of Naples, Italy

Chetan C. Gaonkar^{1, 4}, Diana Sarno¹, Marina Montresor¹,
Carina B. Lange^{1, 2, 3} & Wiebe H.C.F. Kooistra^{1*}

¹ Department of Integrative Marine Ecology, Stazione Zoologica Anton Dohrn, Villa Comunale, 80121 Napoli, Italy

² Departamento de Oceanografía, Universidad de Concepción, Barrio Universitario, Concepción, Chile

³ Centros COPAS Sur-Austral (Universidad de Concepción, Concepción, Chile) and FONDAP-IDEAL (Universidad Austral de Chile, Valdivia, Chile)

⁴ Texas A&M University, O&M Building, College Station, Texas 77843, USA

* Corresponding author: kooistra@szn.it

With 18 figures and 1 table

Abstract: In the present study we describe and illustrate a new species in the genus *Chaetoceros*, *C. turingii* sp. nov., from the Gulf of Naples, Italy. Colonies have a brush-like appearance due to the apparent randomness in seta orientation. The defining feature of this species is the regular pattern of narrow ridges on the exterior of the terminal valve face, which is visible in electron microscopy. In addition, a petal-like collar is present at the base of each intercalary seta. Its nuclear-encoded 18S rDNA and partial 28S rDNA sequences were resolved in a clade with *C. anastomosans*, *C. dayaensis*, *C. cf. vixibilis* as well as with three other *Chaetoceros* species still in need of description. The new species is compared with morphologically similar species, and their differences are discussed.

Keywords: *Chaetoceros turingii* sp. nov.; morphology; Turing pattern; molecular phylogeny; 18S rDNA; 28S rDNA; Gulf of Naples

Introduction

Chaetoceros Ehrenberg is an abundant and diverse diatom genus in the marine phytoplankton (e.g. Guiry & Guiry 2018; Malviya et al. 2016). Its defining feature is the siliceous tubular structures, called setae, protruding from the corners of the valves (generally two setae per valve). Species are characterised based on the morphology of their vegetative cells and chains, shape, number and location of their plastids, orientation and shape of their setae (Hasle & Syvertsen 1997), and ultrastructure of their cell wall elements, comprising valves, girdle bands, and setae (e.g. Lee et al. 2014a, 2014b). Many species form resting spores, which also exhibit a wealth of morphological and ultrastructural characters for species identification (Ishii 2017). The genus is taxonomically well-studied with many species new to science being described frequently (e.g. Balzano et al. 2017; Gaonkar et al. 2017, 2018; Kooistra et al. 2010; Li et al. 2013, 2015, 2017; Xu et al. 2018).

Recently, Gaonkar et al. (2018) characterised numerous monoclonal strains of *Chaetoceros*. Several of these did not match any known species. Two strains, Na26C1 and Na28A1, from specimens collected in the Gulf of Naples in early fall of 2014, shared identical 18S and partial 28S rDNA sequences and were described provisionally as *Chaetoceros* sp. Clade Na28A1. These sequences were resolved in a clade with *C. dayaensis* Y. Li & S. Zhu (Li et al. 2015),

C. anastomosans Grunow and *C. cf. vixvisibilis* Schiller (De Luca et al. 2019b; Gaonkar et al. 2018).

In the present study, we describe the cell morphology and frustule ultrastructural details of the two strains (Na26C1 and Na28A1) as a new species, *Chaetoceros turingii* sp. nov., and compare it with similar species in the genus. What makes *C. turingii* sp. nov. unique among *Chaetoceros* species known so far, is the presence of ripple-like Turing patterns on the exterior of its terminal valves in a chain. The name refers to Alan M. Turing, who was the first to present a biological explanation for such particular patterns of spots or stripes in biological systems (Turing 1952). Such patterns are recognisable in various ultrastructural details of the diatom frustule, and result from Turing processes during frustule morphogenesis (e.g. Mann 2006; Willis et al. 2013).

This paper is dedicated to Richard (Dick) M. Crawford whose pioneering work in electron microscopy to study various aspects of diatoms (e.g., Crawford 1974, 1994; Crawford et al. 1990, 1997; Round et al. 1990) has deepened understanding of the diatom frustule and inspired us to explore diatoms as well. The fine details, invisible in light microscopy, provide a better understanding of the incredible diversity of phytoplankton organisms and has, together with molecular information, pushed our knowledge of the form and function way beyond what could be achieved without electron microscopy.

Materials and methods

Strain isolation and maintenance

The strains Na26C1 and Na28A1 were generated from specimens isolated as described in Gaonkar et al. (2018) from a plankton net sample collected at the Long-Term Ecological Research station MareChiara (LTER-MC; 40°48.5'N, 14°15'E) in the Gulf of Naples, Italy, on October 7, 2014. Strains were grown in *f/2* medium (Guillard 1975) prepared using oligotrophic natural seawater added to Guillard's (*f/2*) Marine Water Enrichment Solution (Sigma-Aldrich, St. Louis, USA). Cultures were maintained at 20 °C with 12:12 h Light: Dark (L: D) photoperiod, and at an irradiance of 50 $\mu\text{mol photons m}^{-2} \text{s}^{-1}$ provided by cool white fluorescent light.

Morphological analysis

Light microscopy observations of the cultured strains in exponential growth phase were documented using a Zeiss Axiophot microscope (Carl Zeiss, Oberkochen, Germany) equipped with a Nomarski differential interference contrast, phase contrast, and bright field optics. Micrographs were taken within a few weeks following isolation, using a Zeiss Axiocam HRC digital camera. For scanning and transmission electron microscopy (SEM and TEM), colonies of strain Na28A1 were treated and examined as described in Gaonkar et al. (2017) as modified from Crawford (1994) and Round et al. (1990).

Molecular analysis

The 18S rDNA and partial 28S rDNA sequences of *C. turingii* sp. nov. strain Na26C1 (GenBank # MG972363 and MG921678, respectively) and strain Na28A1 (MG972364 and MG921679) were concatenated and aligned with those of reference sequences of *Chaetoceros* sp. Clade Va7D2 strain Va7D2, *C. anastomosans* strain Na14C3, *C. cf. vixvisibilis* strain Na16A3, *Chaetoceros* sp. Clade Na11C3 strain Na11C3, *Chaetoceros* sp. Clade Na26B1 strain Na26B1 and *C. dayaensis* strain ML107L (only the partial 28S rDNA), as described in Gaonkar et al. (2018). Concatenated sequences of *C. minimus* (Levander) Marino, Giuffrè, Montresor & Zingone strain MC755, *C. thronsdonii* (Marino, Montresor & Zingone) Marino, Montresor & Zingone strain Na44C3 and *Chaetoceros* sp. Clade Na13C2 strain Na13C2 were included as an outgroup. Positions showing ambiguous alignment and gaps in all but one of the sequences were excluded from phylogenetic analyses, and so were introns and the frayed 5'- and 3'-ends of the sequences. Finally, a total of 2405 bp positions were included in the analysis.

Table 1. *Chaetoceros* strains and their GenBank numbers for their SSU and partial LSU rDNA sequences. All strains originated from the LTER MareChiara in the Gulf of Naples, Italy (Gaonkar et al. 2018), except ML107L, which came from Daya Bay, South China Sea, P.R. China (Li et al. 2015).

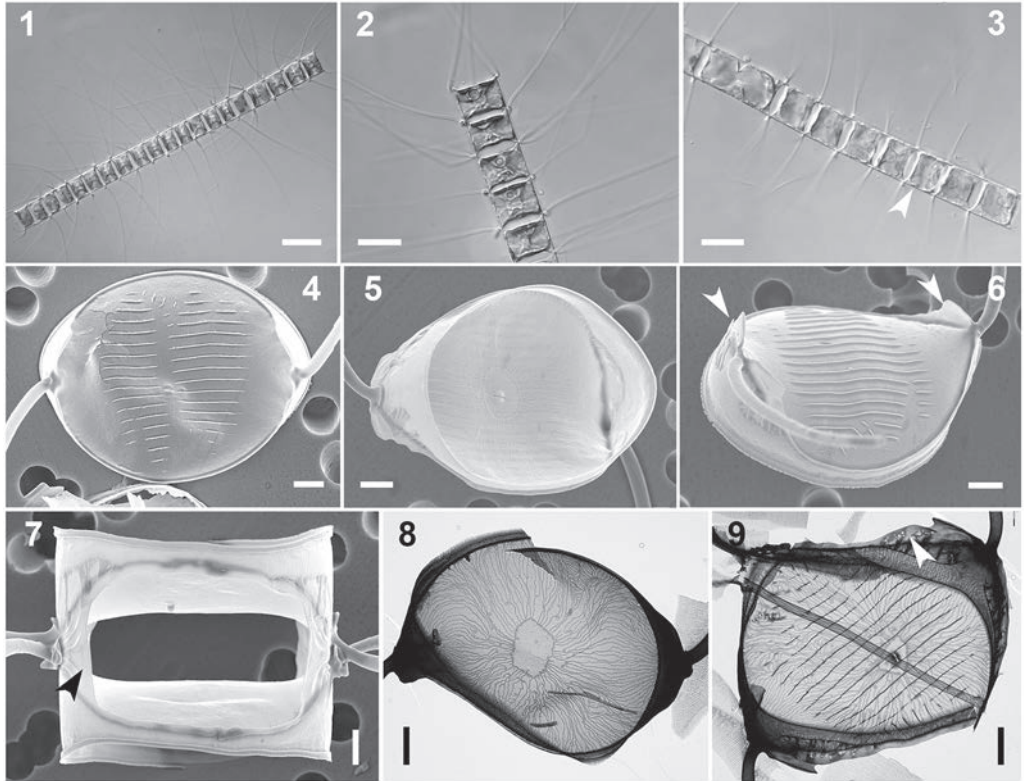
Species	Strain	GenBank # 18S rDNA	GenBank # 28S rDNA
<i>C. anastomosans</i>	Na14C3	MG972359	MG914457
<i>C. dayaensis</i>	ML107L	-	KM401851
<i>C. minimus</i>	MC755	MG972293	MG914570
<i>C. thronsenii</i>	Na44C3	MG972321	MG914631
<i>C. turingii</i> sp. nov.	Na26C1	MG972363	MG921678
<i>C. turingii</i> sp. nov.	Na28A1	MG972364	MG921679
<i>C. cf. vixvisibilis</i>	Na16A3	MG972367	MG914645
<i>Chaetoceros</i> sp. Clade Na11C3	Na11C3	MG972328	MG914605
<i>Chaetoceros</i> sp. Clade Na13C2	Na13C2	MG972344	MG921675
<i>Chaetoceros</i> sp. Clade Na26B1	Na26B1	MG972329	MG914606
<i>Chaetoceros</i> sp. Clade Va7D2	Va7D2	MG972327	MG921670

A maximum likelihood tree was inferred with RAXML as implemented in raxmlGUI v.1.5beta (Silvestro & Michalak 2012), with a GTR-GAMMA base substitution model (values estimated during analysis), a heuristic search (ten-random-additions), rapid hill climbing mode (default) and tree bisection reconnection (TBR) branch swapping. Bootstrap values were obtained with 1000 bootstrap replicates and one random-addition-of-sequences run per bootstrap replicate (thorough bootstrap analysis). A GTR model of base substitutions was estimated during analysis with rate matrix: A↔C (0.9086), A↔G (2.7593), A↔T (1.3983), C↔G (0.9389), C↔T (4.9628), relative to G↔T (1.0000), a gamma-distributed rate variation among sites with shape parameter $\alpha = 0.1568$, and estimated base frequencies: A= 0.274, C= 0.189, G= 0.265, T= 0.272.

A Bayesian tree was inferred with MrBayes 3.2.2 on XSEDE (Ronquist & Huelsenbeck 2003) using the default-value of four Markov chains and a ‘temperature’ parameter of 0.2. The Monte Carlo Markov Chain (MCMC) length was set at one million generations, with a posterior probability of bipartitions sampled every 100 generations and diagnosed every 1000 generations. The BPP values were stabilised just before 1500 trees were gathered. The initial 1500 trees were discarded as burn-in. BI-consensus trees and BPP values were obtained from the retained 8500 trees. A GTR model of base substitutions was estimated during analysis with rate matrix: A↔C (0.0761), A↔G (0.2313), A↔T (0.1168), C↔G (0.0778), C↔T (0.4145) relative to G↔T (0.0836), a gamma-distributed rate variation among sites with shape parameter $\alpha = 17.0250$, a proportion of invariable sites 0.5784, and estimated base frequencies: A= 0.271, C= 0.191, G= 0.266, T= 0.270. The posterior probabilities of the 8501 sampled BI-trees showed a standard deviation of 0.017.

Results

The strains Na26C1 and Na28A1 were found to belong to one and the same species. Their partial 28S rDNA sequences were identical and so were their 18S rDNA sequences. They were morphologically identical as well, except that at the time LM pictures were taken, cells of Na28A1 were slightly narrower in broad girdle view than those of Na26C1. This may have resulted merely from a different number of mitotic cell divisions following sexual reproduction.



Figs 1–17. *Chaetoceros turingii* sp. nov. strains Na26C1 (Figs 1 & 2) and Na28A1 (Figs 3–17).

Fig. 1. Cell colony in broad girdle view (LM). Scale bar = 50 μm. **Fig. 2.** Part of a colony in broad girdle view (LM) showing lobed plastid containing one or two pyrenoids. Scale bar = 20 μm. **Fig. 3.** Part of cell colony in broad girdle view (LM). Note the slight constriction between mantle and girdle. Arrow points to constriction between mantle and girdle band. Scale bar = 20 μm. This figure represents the holotype. **Fig. 4.** Terminal valve, exterior valve view (SEM) showing central rimoportula opening and the valve face ornamented with a regular pattern of narrow ridges (Turing pattern). Scale bar = 2 μm. **Fig. 5.** Terminal valve, interior valve view (SEM), showing central rimoportula; the narrow lines correspond to the external ridges. Scale bar = 2 μm. **Fig. 6.** Terminal valve, exterior valve view (SEM). Arrows point to the silica ridge at the edge between valve face and mantle and the wing-like rims flanking the base of the setae at the valve apices. Scale bar = 2 μm. **Fig. 7.** Sibling intercalary valves, exterior girdle view (SEM). Arrow points to the overlapping silica membrane between the sibling valves. Scale bar = 2 μm. **Fig. 8.** Intercalary valve, interior view (TEM) showing central annulus and radiating costae. Scale bar = 2 μm. **Fig. 9.** Terminal valve, interior view (TEM) showing central annulus with rimoportula, radiating costae and narrow ridges. Arrow points to the wing-like rims flanking the base of the setae. Scale bar = 2 μm.

We report these strains here as belonging to a new species *Chaetoceros turingii* sp. nov. based on our morphological and phylogenetic results. Morphology of vegetative cells and ultrastructural details of frustule elements are described below based on culture material.

Chaetoceros turingii Kooistra & Sarno sp. nov. (Figs 1–17)

Diagnosis: Colonies straight; cells rectangular in broad girdle view. Apertures lanceolate. Single

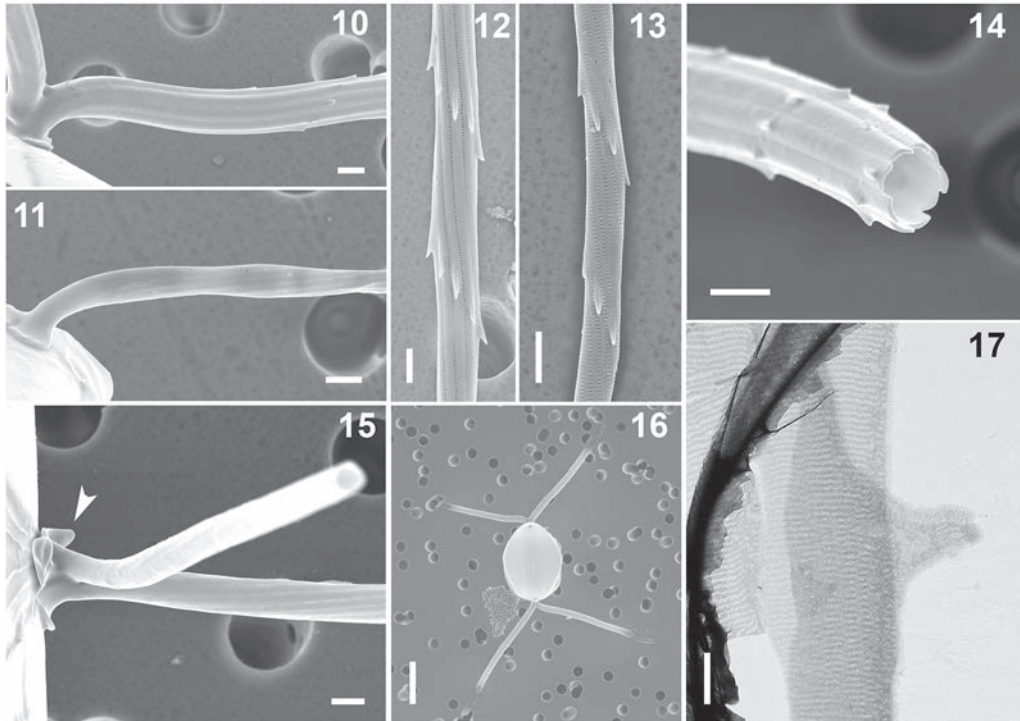


Fig. 10. Sibling intercalary valves, basal part of intercalary setae (SEM). Scale bar = 1 μ m. **Fig. 11.** Terminal seta basal part (SEM). Scale bar = 1 μ m. **Fig. 12.** Intercalary seta in distal part (SEM). Scale bar = 1 μ m. **Fig. 13.** Terminal seta in distal part (SEM). Scale bar = 1 μ m. **Fig. 14.** Intercalary seta in cross section (SEM). Scale bar = 1 μ m. **Fig. 15.** Basal part of intercalary setae with petal-like collar (SEM). Arrow points to the petal-like collar. Scale bar = 1 μ m. **Fig. 16.** Internal view of intercalary valve with broad V-shaped setae (SEM). Scale bar = 10 μ m. **Fig. 17.** Detail of circular band (TEM). Scale bar = 1 μ m.

lobed plastid with one or two pyrenoids. Terminal valves with small central rimoportula in annulus; their exterior valve face ornamented with narrow ridges, parallel with apical axis. Setae robust, circular in cross section, ornamented beyond basal part with shark fin-shaped spines, transversely elongated poroids at regular intervals, and irregularly spaced larger pores. Terminal setae oriented in narrow U shape. Intercalary setae with petal-like collar at their base. Girdle bands with transverse costae and perforated with minute pores.

Holotype: A permanent slide of strain Na28A1, isolated from Gulf of Naples, Italy, deposited at the Museum of the Stazione Zoologica Anton Dohrn, Naples, Italy, as no. SZN-Na28A1. Fig. 3 represents the holotype.

Isotype: SEM stubs, TEM grids and fixed material of strain Na28A1, isolated from the Gulf of Naples, Italy, deposited at the Museum of Stazione Zoologica Anton Dohrn, Naples, Italy.

Type locality: Long-Term Ecological Research station MareChiara (LTER-MC 40°48.5'N 14°15'E), Gulf of Naples, Italy.

Habitat: Marine planktonic.

Etymology: The species epithet “turingii” refers to the presence of a Turing pattern on the terminal valves and as a credit to Alan M. Turing who described these patterns mathematically in “The Chemical Basis of Morphogenesis” (Turing, 1952; see also Kondo & Miura, 2010).

Morphology and ultrastructure: Colonies consist of straight to slightly bent chains that, in rapidly growing cultures, can be up to 20 cells long (Figs 1–3). Cells rectangular in broad girdle view, each with a single, lobed plastid containing one or two conspicuous pyrenoids (Fig. 2). Apertures between sibling cells are oblong to lanceolate, at times slightly constricted in the central part (Fig. 2). Cells measure 14–25 μm in broad girdle view, 16–24 μm at the perivalvar axis (Figs 1–3). The height of the mantle corresponds to about one third of the cell height along the perivalvar axis (Fig. 3). Setae long, protruding from the elevated valve apices. Intercalary setae cross at the chain margin and proceed in all directions, giving the colony a dishevelled, bushy appearance (Figs 1–3). Terminal setae oriented in a U shape, at times crossing each other in the distal part (Fig. 2). Solitary cells were not observed, and neither were resting spores.

Valves are broadly elliptical in shape (Figs 4 & 5). The valve face is saddle-shaped (Fig. 6), at times slightly raised in the central part. The edge between valve face and mantle is arc-shaped and exhibits a silica ridge, which is diminutive in the middle part, to become more pronounced towards the valve apices, extending into wing-like hyaline rims (Figs 4–6) flanking the base of the setae at the valve apices and connecting with the ones of the sibling valves (Fig. 7).

Costae on the valve face diverge from a central to slightly pericentral, irregularly shaped annulus. They ramify irregularly, and continue in the mantle (Figs 8 & 9). Costae converge towards the valve apices (Figs 8 & 9). At times, costae emerge from a spiral-shaped origin (Figs 8 & 9). The central part of the exterior valve face in terminal valves is ornamented with narrow ridges equidistantly from one another, oriented more or less in parallel with the apical axis (Figs 4, 6 & 9). A small central rimoportula is present on the terminal valve, inside the annulus (Figs 4–6 & 9). There are no poroids between the costae (Figs 8 & 9).

Terminal and intercalary setae have similar ultrastructure; their proximal part is robust, without any ornamentation or perforation (Figs 10 & 11), and setae become thinner distally (Figs 12 & 13). Setae are circular in cross section (Fig. 14). They are ornamented with regularly spaced, shark fin-shaped spines and poroids arranged in a spiral pattern, and slightly larger pores at irregular intervals (Figs 12 & 13). Intercalary setae exhibit a petal-like collar at their base (Figs 7 & 15). They fuse briefly with their sibling setae at the chain margin, and then abruptly bend away from each other in a wide V-shape in valve view (Fig. 16) and narrow V-shape in broad girdle view (Fig. 15).

Girdle bands are open and exhibit transverse parallel costae with numerous minute poroids (Fig. 17).

Distribution. *Chaetoceros turingii* sp. nov. has been recorded in the plankton of the Gulf of Naples.

Molecular characterisation. The species is defined by the combined nucleotide sequences of strain Na28A1: D1-D3 of 28S rDNA (GenBank # MG921679) and the full length 18S rDNA (GenBank # MG972364).

Phylogenetic trees inferred from the concatenated sequences. The maximum likelihood (ML) and Bayesian inference (BI) trees showed the same topology; only the ML tree is shown (Fig. 18). The first taxa to branch off were *Chaetoceros* sp. Clade Va7D2 strain Va7D2 and *C. dayaensis* strain MC107L. Then followed by strains Na26C1 and Na28A1 of *C. turingii* sp. nov., which is sister to a clade with *C. anastomosans* strain Na14C3, *C. cf. vixvisibilis* strain Na16A3 and *Chaetoceros* spp. Clade Na26B1 strain Na26B1 and Clade Na11C3 strain Na11C3.

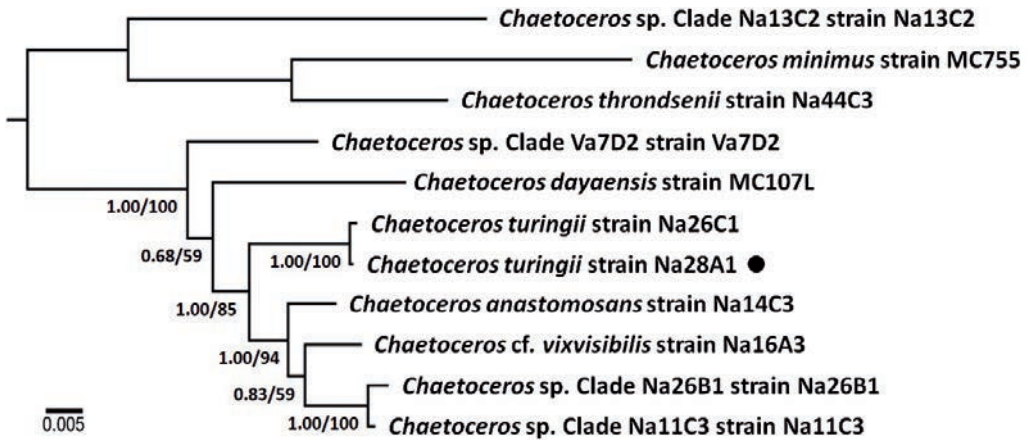


Fig. 18. Maximum likelihood tree (-ln L = 6031.9862) inferred from the concatenated sequences of the partial 28S and entire 18S rDNA sequences of *Chaetoceros* strains recovered in Clade VIIc of Gaonkar et al. (2018). Sequences of *C. minimus* strain MC755, *C. throndsenii* strain Na44C3 and *Chaetoceros* sp. Clade Na13C2 strain Na13C2 were used as outgroup. Bayesian posterior probabilities (BI) and bootstrap values (ML) are indicated (BI/ML) at their respective internodes of the ingroup the black dot indicates the strain from which the holotype has been taken.

Discussion

The distinctive feature of *C. turingii* sp. nov. constitutes the Turing pattern of narrow ridges on the terminal valve exterior, oriented more or less in parallel with the apical axis. As far as is known to us, none of the other *Chaetoceros* species possess this particular pattern.

We did not observe resting spores in our cultures of the two strains of *C. turingii* sp. nov. In the case of closely related species, which often share highly similar vegetative morphology, spores are helpful in identifying species, since these cells often differ markedly in the ultrastructural details of their ornamentation (see e.g. Gaonkar et al. 2017; Li et al. 2017). Unfortunately, spores are not always reported in taxonomic studies of *Chaetoceros* because conditions under which they form are not clarified and seem to differ among species.

Phylogenetically, *C. turingii* sp. nov. belongs to a lineage of taxa referred to as Clade VIIc in Gaonkar et al. (2018) and is composed of relatively delicate species including *C. anastomosans*, *C. cf. vixvisibilis*, *C. dayaensis* and three undescribed taxa for which morphological information is available. All the species in the ingroup share the irregularly ramifying costae in the valve face, the irregularly shaped annulus, the absence of poroids between the costae in the valves and the general seta orientation (Bosak & Sarno 2017; Gaonkar et al. 2018; Hernández-Becerril et al. 2010; Li et al. 2015) as described for *C. turingii* sp. nov. Except in *C. anastomosans*, the sibling intercalary setae cross over and then bend immediately in a wide V-shape in the valvar plane and in a narrow V-shape in the apical plane. Pairs of terminal setae initially bend in opposite directions and then curve in a U-shape parallel with the perivalvar axis. The short, basal part of the setae is round without any perforations.

A comparison with the close relatives of *C. turingii* sp. nov. shows various morphological differences. None of these species show the Turing pattern on their terminal valves. *Chaetoceros dayaensis* shares with the new species the wing-like expansions flanking the base of the setae and the shark fin-shaped spines on the setae (Li et al. 2015). However, their setae differ markedly; the longitudinal ribs in the setae of *C. dayaensis* do not spiral; terminal setae are hexagonal in

cross section and more robust than the quadrangular intercalary ones. Intercalary setae cross over just outside the valve margin (Li et al. 2015). Also, the aperture appears to be much wider. The ultrastructure of the terminal and intercalary setae in *Chaetoceros* sp. Clade Va7D2 (Gaonkar et al. 2018) are comparable to those of *C. dayaensis*, in terms of dimorphy. Its intercalary setae cross over outside the valve margin. The silica ridge between valve face and mantle is ornamented, at times, with narrow lip-like structures, which link intercalary sibling valves.

Chaetoceros anastomosans shares with *C. turingii* sp. nov. (Gaonkar et al. 2018) the wing-like expansions flanking the base of the setae, and the spiralling of the setae. Yet, intercalary setae do not cross over at their base but link *via* silica bridges well outside the valve margin. Terminal setae are octa- or nonagonal in cross section and more robust than the quadrangular or pentagonal intercalary ones. The shark fin-shaped spines on the setae are minute in comparison with those of *C. turingii* sp. nov.

Chaetoceros sp. Clade Na11C3 is indistinguishable from *C. turingii* sp. nov. in LM. The two share the wings around the seta base, the spiralling setae and the shark fin-shaped spines on the setae. Yet, in EM *Chaetoceros* sp. Clade Na11C3 shows a minute petal-like collar around the base of some of the terminal setae whereas no such collar is present on intercalary setae.

Regarding the species *C. vixvisibilis*, ultrastructural information gathered from Adriatic field material in Bosak & Sarno (2017) and from unpublished field material from the Gulf of Naples reveal that its intercalary setae are basically circular in cross section, composed of 14 or more parallel ribs without any trace of spines. The strain of *C. cf. vixvisibilis* Na18C2 exhibits in LM the typical appearance of this species, but in SEM and TEM its setae are composed of 6-7 parallel ribs and carry spines (Gaonkar et al. 2018), which does not conform to the species *C. vixvisibilis* in Bosak & Sarno (2017).

Several *Chaetoceros* species in the other clades in Gaonkar et al. (2018) form straight chains and exhibit a single plastid per cell, and many among these closely resemble *C. turingii* sp. nov. in LM, as for example, *Chaetoceros* sp. Clade Na12A3 and *Chaetoceros* sp. Clade Na13C2 within Clade VIIa (*C. affinis* and relatives; Gaonkar et al. 2018). Yet, the former two can be distinguished from *C. turingii* sp. nov. in that the basal parts of their terminal and intercalary setae do not bend sharply out of the apical plane, their terminal setae orient in a broad U- or V-shape and their intercalary setae orient more regularly in a narrow V-shape over their entire length, and all setae remain visible in broad valve-view. All the taxa within Clade VIIb (Gaonkar et al. 2018; Li et al. 2013) differ from *C. turingii* sp. nov. in that their intercalary setae proceed for a short distance before fusing briefly in, or just outside, the valve margin. Confusion with members of Clade VIId (*C. lorenzianus* group; Li et al. 2017) is unlikely because these species exhibit multiple plastids per cell, and their setae ultrastructure differs markedly from that observed in *C. turingii* sp. nov. Information of all the aforementioned strains in Gaonkar et al. (2018) is available in that paper's supporting information (descriptions at <https://doi.org/10.1371/journal.pone.0208929.s011> and illustrations in LM, SEM and TEM at <https://doi.org/10.1371/journal.pone.0208929.s012>).

Two additional species, *C. crinitus* Schütt (Schütt 1895) and *C. pseudocrinitus* Ostenfeld (Ostenfeld 1901), resemble *C. turingii* sp. nov. Reference sequences are still lacking for these species and therefore, their phylogenetic position is unknown. Nonetheless, they differ morphologically from *C. turingii* sp. nov. In illustrations of *C. crinitus* in Schütt (1895) and in Grøntved (1950) the setae emerge from inside the valve perimeter, which is not the case in *C. turingii* sp. nov. Ostenfeld's (1901) illustration of *C. pseudocrinitus* (fig. 11) resembles *C. turingii* sp. nov., and so does a strain assigned to *C. pseudocrinitus* by Jensen and Moestrup (1998; LM figs 176, 177; SEM fig. 181; TEM figs 185–187) obtained from the same region as Ostenfeld's material. This strain differs from those of *C. turingii* sp. nov. in that its EM illustrations show a pair of outgrowths near the base of the setae, no Turing patterns in terminal valves, and setae lacking shark fin-shaped spines.

In a revision of the subgeneric classification of the genus *Chaetoceros*, De Luca et al. (2019b) did not put forward a sectional treatment of the Clade VIIc, yet. In the currently accepted treatment, its taxa are placed in different sections: *C. anastomosans* in section *Anastomosantia* Ostenfeld; *C. cf. vixvisibilis* in *Brevicatenata* Gran, and *C. dayaensis* possibly in *Laciniosa* Gran (Li et al. 2015), and the *Chaetoceros* spp. in this clade are not yet assigned (Gaonkar et al. 2018). Therefore, we suggest to refrain from proposing any treatment until the *Chaetoceros* spp. in Gaonkar et al. (2018) have been described formally and the phylogenetic positions of other morphologically similar species, such as e.g., *C. pseudocrinitus*, have been resolved.

Our detection of specimens of *C. turingii* sp. nov. in the plankton of the Gulf of Naples corroborates results of a high throughput sequencing (HTS) V4-18S rDNA metabarcoding study of Chaetocerotaceae, conducted on plankton samples collected over the years 2011–2013 in the Gulf of Naples (Gaonkar et al. 2020), which revealed that the new species is present from late August into October, albeit infrequently. The species is detected also in the V4-18S rDNA metabarcode data generated from samples collected in the Indian River Lagoon, Florida in the frame of Ocean Sampling Day (supplemental information in De Luca et al. 2019a). Its detection in the V9-18S rDNA metabarcode data obtained from a sample taken at an equatorial sample station of TARA Oceans in the Maldives (supplemental information in De Luca et al. 2019a) is unsure because the V9 regions of *C. turingii* sp. nov. and *C. cf. vixvisibilis* are identical (Gaonkar et al. 2018). Although its paucity in these metabarcode data sets does not prove its absence in most geographic locations, the results suggest that the species is uncommon elsewhere as well.

We realize that with the discovery of all these morphologically highly similar and phylogenetically close species, routine monitoring of the diversity in this genus becomes ever more challenging. Nonetheless, once one knows what to look for, the challenge might be overcome. In short, *C. turingii* sp. nov. is a robust species whose terminal valves have a distinctive, and as far as we know, unique ornamentation pattern.

Acknowledgements

The authors thank C. Minucci for assistance with molecular work, F. Tramontano for culture maintenance, A. Manfredonia for medium preparation, the staff of the IRM service in SZN for sampling, A. Graziano, F. Iamunno and G. Lanzotti for assistance with EM, E. Mauriello and R. Pannone for sequencing, and two anonymous reviewers for edits and constructive comments. CCG was supported by a PhD fellowship funded by the SZN (Open University – SZN PhD program). WHCFK acknowledges travel grant from the EU FP7 project ASSEMBLE (Grant Agreement No 227799), and CBL acknowledges partial support by ASSEMBLE and CNRS/LIAMORFUN (Mission No 7569). This study was carried out in the framework of the project FIRB Biodiversitalia (RBAP10A2T4) funded by the Italian Ministry of Education, University and Research (MIUR).

References

- Balzano, S., Percopo, I., Siano, R., Gourvil, P., Chanoine, M., Marie, D., Vaultot, D., & Sarno, D. (2017). Morphological and genetic diversity of Beaufort Sea diatoms with high contributions from the *Chaetoceros neogracilis* species complex. *Journal of Phycology* 53(1), 161–187.
- Bosak, S., & Sarno, D. (2017). The planktonic diatom genus *Chaetoceros* Ehrenberg (Bacillariophyta) from the Adriatic Sea. *Phytotaxa* 314(1), 1–44.
- Crawford, R. M. (1974). The auxospore wall of the marine diatom *Melosira nummuloides* (Dillw.) C. Ag. and related species. *British Phycological Journal* 9(1), 9–20.
- Crawford, R. M. (1994). Transmission electron microscopy and diatom research. Proceedings of the 11th IDS, San Francisco, 1990. *Memoirs of the California Academy of Sciences* 17, 5–19.
- Crawford, R. M., Sims, P. A., & Hajos, M. (1990). The morphology and taxonomy of the centric diatom genus *Paralia* 1. *Paralia siberica* comb. nov. *Diatom Research* 5(2), 241–252.

- Crawford, R. M., Hinz, F., & Rynearson, T. (1997). Spatial and temporal distribution of assemblages of the diatom *Corethron criophilum* in the polar frontal region of the South Atlantic. *Deep-Sea Research Part II: Tropical Studies in Oceanography* 44(1-2), 479–496.
- De Luca, D., Kooistra, W. H. C. F., Sarno, D., Gaonkar, C. C., & Piredda, R. (2019a). Global distribution and diversity of *Chaetoceros* (Bacillariophyta, Mediophyceae): integration of classical and novel strategies. *PeerJ* 7, e7410.
- De Luca, D., Sarno, D., Piredda, R., & Kooistra, W. H. C. F. (2019b). A multigene phylogeny to infer the evolutionary history of Chaetocerotaceae (Bacillariophyta). *Molecular Phylogenetic Evolution* 140, 106575.
- Gaonkar, C. C., Kooistra, W. H. C. F., Lange, C. B., Montresor, M., & Sarno, D. (2017). Two new species in the *Chaetoceros socialis* complex (Bacillariophyta): *C. sporotruncatus* and *C. dichatoensis*, and characterization of its relatives, *C. radicans* and *C. cinctus*. *Journal of Phycology* 53, 889–907.
- Gaonkar, C. C., Piredda, R., Minucci, C., Mann, D. G., Montresor, M., Sarno, D., & Kooistra, W. H. C. F. (2018). Annotated 18S and 28S rDNA reference sequences of taxa in the planktonic diatom family Chaetocerotaceae. *PLoS ONE* 13(12), e0208929. <https://doi.org/10.1371/journal.pone.0208929>.
- Gaonkar, C. C., Piredda, R., Sarno, D., Zingone, A., Montresor, M., & Kooistra, W. H. C. F. (2020). Species detection and delineation in the marine planktonic diatoms *Chaetoceros* and *Bacteriastrum* through metabarcoding: making biological sense of haplotype diversity. *Environmental Microbiology* 22, 1917–1929. <https://doi.org/10.1111/1462-2920.14984>
- Grøntved, J. (1950). The phytoplankton of Præstø Fjord. *Folia Geographica Danica* 3, 154–169.
- Guillard, R. R. L. (1975). Culture of phytoplankton for feeding marine invertebrates. In W. L. Smith, & M. H. Chanley (eds.), *Culture of marine invertebrate animals* (pp. 29–60). New York: Plenum Press.
- Guiry, M. D., & Guiry, G. M. (2018). *AlgaeBase*. World-wide electronic publication, National University of Ireland, Galway. Available from <http://www.algaebase.org>
- Hasle, G. R., & Syvertsen, E. E. (1997): Marine diatoms. In C. R. Tomas (ed.), *Identifying marine phytoplankton* (pp. 5–385). San Diego: Academic Press.
- Hernández-Becerril, D. U., Viličić, D., Bosak, S., & Djakovac, T. (2010). Morphology and ecology of the diatom *Chaetoceros vixvisibilis* (Chaetocerotales, Bacillariophyceae) from the Adriatic Sea. *Journal of Plankton Research* 32, 1513–1525.
- Ishii, K.-I. (2017). Morphology and species identification of *Chaetoceros* species (Bacillariophyceae). *Perspectives in Phycology* 4, 61–71.
- Jensen, K. G. & Moestrup, Ø. (1998). The genus *Chaetoceros* (Bacillariophyceae) in inner Danish coastal waters. *Opera Botanica* 133, 5–68.
- Kooistra, W. H. C. F., Sarno, D., Hernandez Becerril, D. U., Assmy, P., DiPrisco, C., & Montresor, M. (2010). Comparative molecular and morphological phylogenetic analyses of taxa in the Chaetocerotaceae (Bacillariophyta). *Phycologia* 49, 471–500.
- Kondo, S. & Miura, T. (2010). Reaction-diffusion model as a framework for understanding biological pattern formation. *Science* 329, 1616–1620.
- Lee, S. D., Park, J. S., Yun, S. M., & Lee, J. H. (2014a). Critical criteria for identification of the genus *Chaetoceros* (Bacillariophyta) based on setae ultrastructure. I. Subgenus *Chaetoceros*. *Phycologia* 53(2), 174–187.
- Lee, S. D., Joo, H. M., & Lee, J. H. (2014b). Critical criteria for identification of the genus *Chaetoceros* (Bacillariophyta) based on setae ultrastructure. II. Subgenus *Hyalochaete*. *Phycologia* 53(6), 614–638.
- Li, Y., Boonprakob, A., Gaonkar, C. C., Kooistra, W. H. C. F., Lange, C. B., Hernández-Becerril, D., . . . Lundholm, N. (2017). Diversity in the globally distributed diatom genus *Chaetoceros* (Bacillariophyceae): three new species from warm-temperate waters. *PLoS ONE* 12(1). doi: 10.1371/journal.pone.0168887
- Li, Y., Lundholm, N., & Moestrup, Ø. (2013). *Chaetoceros roto sporus* sp. nov. (Bacillariophyceae), a species with unusual resting spore formation. *Phycologia*. 52, 600–608.
- Li, Y., Zhu, S., Lundholm, N., & Lü, S. (2015). Morphology and molecular phylogeny of *Chaetoceros dayaensis* sp. nov. (Bacillariophyceae), characterized by two 90° rotations of the resting spore during maturation. *Journal of Phycology* 51, 469–479.
- Malviya, S., Scalco, E., Audic, S., Vincent, F., Veluchamy, A., Poulain, J., . . . Bowler, C. (2016). Insights into global diatom distribution and diversity in the world’s ocean. *Proceedings of the National Academy of Sciences USA* 113, E1516–E1525.
- Mann, D. G. (2006). Specifying a morphogenetic model for diatoms: an analysis of pattern faults in the Voigt zone. *Nova Hedwigia, Beiheft* 130, 97–118.

- Ostenfeld, C. H. (1901). Jagttagelser over Plankton-Diatomeer. *Nyt Magazin Naturvidenskaberne* 39, 287–302.
- Ronquist, F., & Huelsenbeck, J. P. (2003). MrBayes 3: Bayesian phylogenetic inference under mixed models. *Bioinformatics* 19, 1572–1574.
- Round, F. E., Crawford, R. M., & Mann, D. G. (1990), *The diatoms. Biology & morphology of the genera*. Cambridge: University Press.
- Schütt, F. (1895). Arten von *Chaetoceras* und *Peragallia*. Ein Beitrag zur Hochseeflora. *Bericht der Deutschen Botanischen Gesellschaft* 13, 35–50.
- Silvestro, D., & Michalak, I. (2012): raxmlGUI: a graphical front-end for RAxML. *Organisms Diversity & Evolution* 12, 335–337.
- Turing, A. M. (1952). The chemical basis of morphogenesis. *Philosophical Transactions of the Royal Society B, Biological Sciences* 237, 37–72.
- Willis, L. Cox, E. J., & Duke, T. (2013). A simple probabilistic model of submicroscopic diatom morphogenesis. *Journal of the Royal Society Interface* 10(83), 1–9.
<https://doi.org/10.1098/rsif.2013.0067>
- Xu, X. J., Chen, Z. Y., Lundholm, N., & Li, Y. (2018). Revisiting *Chaetoceros subtilis* and *C. subtilis* var. *abnormis* (Bacillariophyceae), reinstating the latter as *C. abnormis*. *Phycologia* 57, 659–673.

